PART 5

MAGNETIC FIELDS AND INFRARED MAGNETOMETRY

https://doi.org/10.1017/S0074180900124659 Published online by Cambridge University Press

VECTOR MAGNETOMETRY USING THE 12-μm EMISSION LINES

D. DEMING
Code 693, NASA/Goddard Space Flight Center, Greenbelt, MD 20771, U.S.A.
T. HEWAGAMA
Hughes/STX Corporation, 4400 Forbes Boulevard, Lanham, MD 20706, U.S.A.
D. E. JENNINGS
Code 693, NASA/Goddard Space Flight Center, Greenbelt, MD 20771, U.S.A.
G. McCABE
Hughes/STX Corporation, 4400 Forbes Boulevard, Lanham, MD 20706, U.S.A.
and
G. WIEDEMANN
European Southern Observatory, Karl-Schwarzschildstrasse 2, D-8046 Garching bei München, Germany

Abstract. Recent polarimetric observations of the 12.32-μm emission line have provided the observational basis for deriving vector magnetic fields in the upper photosphere with great sensitivity. We use a line source function from the non-LTE model of Carlsson, Rutten and Shchukina, and calculate the radiative transfer of the Stokes I, Q, U, and V profiles. The results show that the profiles are not significantly affected by magneto-optical effects or by saturation, and reliable vector fields can be extracted by simply fitting the Seares relations to the Stokes profiles. Vector field observations for sunspots have shown that the field extends well beyond the photometric boundary of the sunspot, but that the field strength at the penumbral/photospheric boundary is less than half of the sunspot-center value. Within a mature sunspot, the 12-μm line profiles contain essentially no unpolarized radiation, indicating that the field is not intermittent in the sense of containing discrete flux tubes separated by field-free regions. We describe the design of a 12-μm Stokes polarimeter incorporating a high-resolution Fabry-Perot etalon and a 128 × 128 infrared array detector.

Key words: infrared: stars – instrumentation: polarimeters – line formation – Sun: magnetic fields

1. Introduction

The Mg I emission lines near 12 μm are the most magnetically-sensitive lines which can currently be observed in the solar spectrum, and are of great interest in studies of solar magnetic and electric fields (Deming *et al.* 1988; Chang and Schoenfeld 1991). The well-understood nature of the atomic physics (Chang 1993) and the recent development of convincing NLTE formation theories for these lines (Chang *et al.* 1991, Carlsson, Rutten and Shchukina 1992, hereafter CRS), in combination with limb measurements at the 1991 total eclipse (Jennings *et al.* 1993), lay a firm foundation for their diagnostic use.

We now understand that the lines are formed in the upper photosphere, several pressure scale heights above the regions sensed in visible magnetograms. Most magnetic observations have utilized the Mg I line at 12.32 μm. CRS have given the line-center contribution function for this transition, showing that it peaks near $\log(\tau_{500}) = -2.7$, whereas a typical visible-region photospheric line senses the region near $\log(\tau_{500}) = -1.0$, (see, *e.g.*, Rees, Murphy and Durrant 1989). While this difference in formation level is quite modest, it occurs over an important regime.

D. M. Rabin et al. (eds.), Infrared Solar Physics, 379–392.

https://doi.org/10.1017/S0074180900124659 Published online by Cambridge University Press

Consulting model atmospheres (*e.g.*, Maltby *et al.* 1986), we find that the ratio of external gas pressure to the magnetic pressure of a 1,000-Gauss field is 0.1 at the 12-μm height, versus a value near unity for a typical visible photospheric line. This change from the regime where gas and magnetic pressures are comparable, to the regime where magnetic pressure dominates, is of considerable physical significance. Simultaneous magnetic observations at 1.6 μm (Rabin 1992) and 12 μm would be especially interesting, because the significant difference in the gas-to-magnetic pressure ratio would be accompanied by the large magnetic splitting which is characteristic of infrared (IR) lines.

Vector magnetometry using the 12-μm lines requires both polarimetric observations and the means to interpret them and extract the magnetic vector. The capability to make polarimetric 12-μm observations using the McMath Fourier transform spectrometer (FTS) was developed by Hewagama (1991), and Hewagama *et al.* (1992). The polarization properties of the McMath telescope are quite favorable at this long wavelength and the observations do not require correction for telescope polarization (Hewagama 1991; Deming *et al.* 1991). The greatest observational limitation at present is the single-detector nature of the FTS observations. We have recently begun to use array detectors for 12-μm observations, and we will here describe the methodology of the observations and progress toward constructing a 12-μm Stokes polarimeter using a 2-D IR array detector.

As concerns the extraction of vector fields, we need to evaluate the impact of the NLTE models. Hewagama (1991) assumed that the emission was optically thin and derived vector fields by fitting the Seares (1913) relations to the observed Stokes profiles. The assumption of optical thinness should be re-examined in the light of the new models, which show line-center optical depths reaching values greater than unity. We have therefore calculated theoretical Stokes profiles for the 12.32-μm line based on the CRS model results, and we will show that the Hewagama (1991) fits to the Seares (1913) relations are quite adequate for the purpose of extracting the field vector.

2. Quantum Mechanics of the Transition

The 12-μm lines were identified by Chang and Noyes (1983), and Chang (1987, 1992) has discussed the quantum mechanics of the transitions. We here reiterate and expand on a few aspects of the 12.32-μm line which are especially relevant to vector field determinations. The upper state has $n = 7$, $l = 6$ and the lower state $n = 6$, $l = 5$. Fine structure due to spin-orbit coupling is quite small, of order 0.0005 cm^{-1}, much less than the quiet-Sun line width of 0.017 cm^{-1}.

Figure 1 (from Hewagama 1991) shows the level configurations for the line calculated using the Chang (1987) formulae and assuming that the atom is immersed in a 300 Gauss external magnetic field. In the presence of even this relatively weak magnetic field, the interaction energy of the total angular momentum vector with the magnetic field is larger than the spin-orbit fine structure. The total angular momentum in the field direction is m in Figure 1, and spin-orbit interaction produces the fine structure at each m. The transitions $\Delta m = 0$ produce the π component in the "Zeeman" pattern, while $\Delta m = \pm 1$ produce the σ components. Figure 2

https://doi.org/10.1017/S0074180900124659 Published online by Cambridge University Press

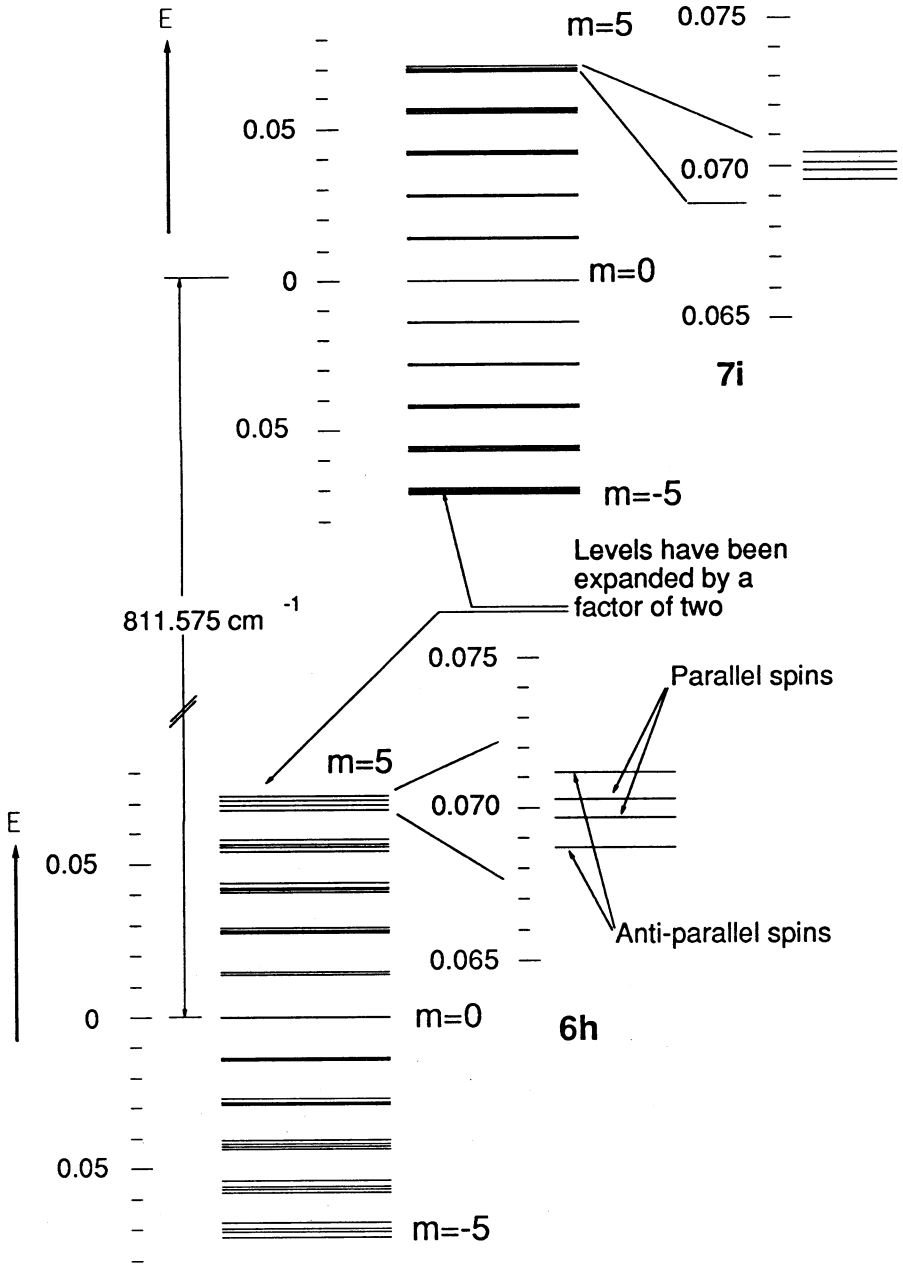

Fig. 1. Energy level diagram for the 12.32-μm line. The $m = 6$ states in the upper level are not illustrated.

https://doi.org/10.1017/S0074180900124659 Published online by Cambridge University Press

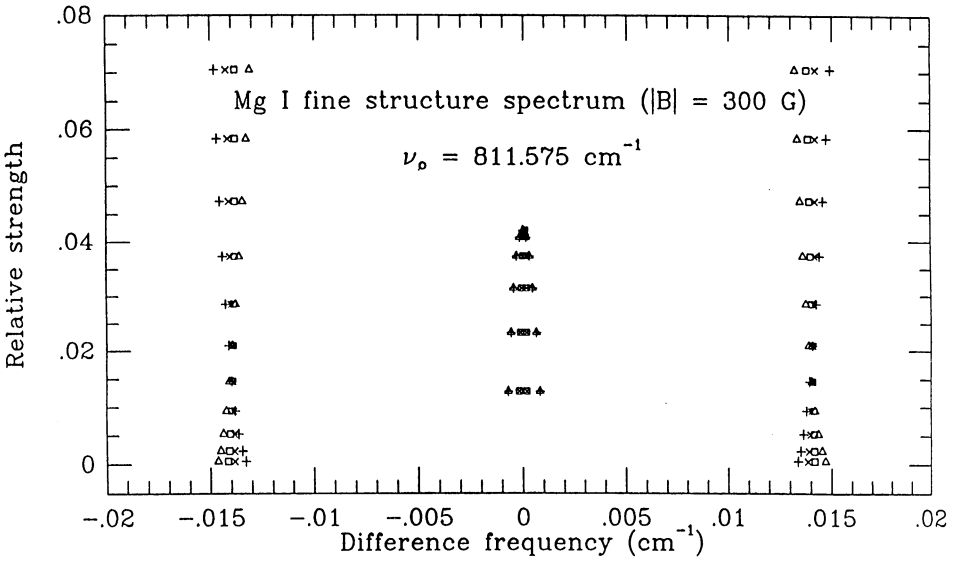

Fig. 2. Positions and relative strengths of "Zeeman" components in the 12.32-μm line spectrum for a 300-Gauss magnetic field strength.

shows the resultant "Zeeman" pattern, with fine structure in the components being significantly less than the splitting. Solar active-region magnetic fields observed in this line to date are seldom much weaker than 300 Gauss. Consequently, the line can be well approximated as a normal Zeeman triplet having Landé-g factor of unity (Chang 1987), and the fine structure in each component can be ignored. For truly weak fields (tens of Gauss or less) the fine structure in the magnetic pattern would have to be accounted for.

3. Radiative Transfer and the Stokes Profiles

Figure 3 shows an example of Stokes profiles observed for this line by Hewagama *et al.* (1992), in comparison with profiles calculated using the Seares relations. The Seares fit assumes that the line components are Gaussian emissions having widths equal to the observed profiles. They were fit to the observations using non-linear least squares, resulting in the field strength, $|\mathbf{B}|$, line-of-sight inclination, γ, and azimuth, α, shown in the I profile (upper left panel) in the Figure. The assumption underlying the Seares fit is that the emission components are optically thin, *i.e.*, that photons emitted upward from the upper state progress without significant re-absorption. Departures from optical thinness could, in principle, affect the fits in two ways. First, the ratio of amplitudes in the π and σ components, which indicates the inclination to the line-of-sight, could be affected by saturation. In the case where the line is very optically thick, the central intensities in the π and σ components will all approach the value of the source function in the line-forming

https://doi.org/10.1017/S0074180900124659 Published online by Cambridge University Press

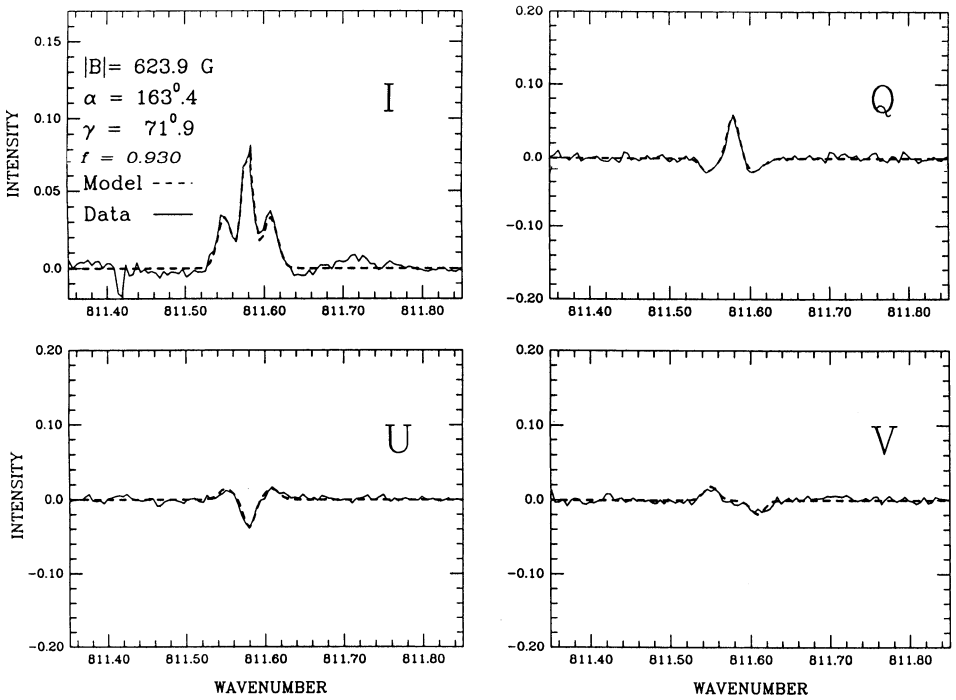

Fig. 3. Observed Stokes profiles of the 12.32 μm lines in a sunspot penumbra (solid line), in comparison to a fit of the Seares formulae (dashed line). The derived field strength and orientation are noted, as well as the fractional polarization, *i.e.*, the fraction (f) of the emission in Stokes I which is accounted for by the polarized light intensity, $\sqrt{Q^2 + U^2 + V^2}$.

region of the photosphere, relatively independent of the field inclination. Second, the Stokes profiles can, in principle, exhibit magneto-optical effects, where line absorption results in conversion of one polarization state to another (*e.g.*, from linear to circular).

To test whether these two possibilities are important in practice, we have calculated Stokes I, Q, U and V profiles for this line using a more rigorous radiative transfer approach. We adopted the CRS line-center source function, and used a Voigt profile for the line. The Doppler width for the line was taken to be 0.017 cm^{-1} FWHM, the same as the observed line. The damping parameter was taken to be proportional to gas pressure, and the constant of proportionality was adjusted to reproduce the absorption wings which are present on the observed quiet-Sun line. We used the DELO method described by Rees, Murphy and Durrant (1989), and we checked our implementation of the method by comparing to the results of a direct quadrature integration of the Stokes radiative transfer equations. The DELO calculations included magneto-optic effects.

Figure 4 (left) shows DELO profiles computed with and without magneto-optics.

https://doi.org/10.1017/S0074180900124659 Published online by Cambridge University Press

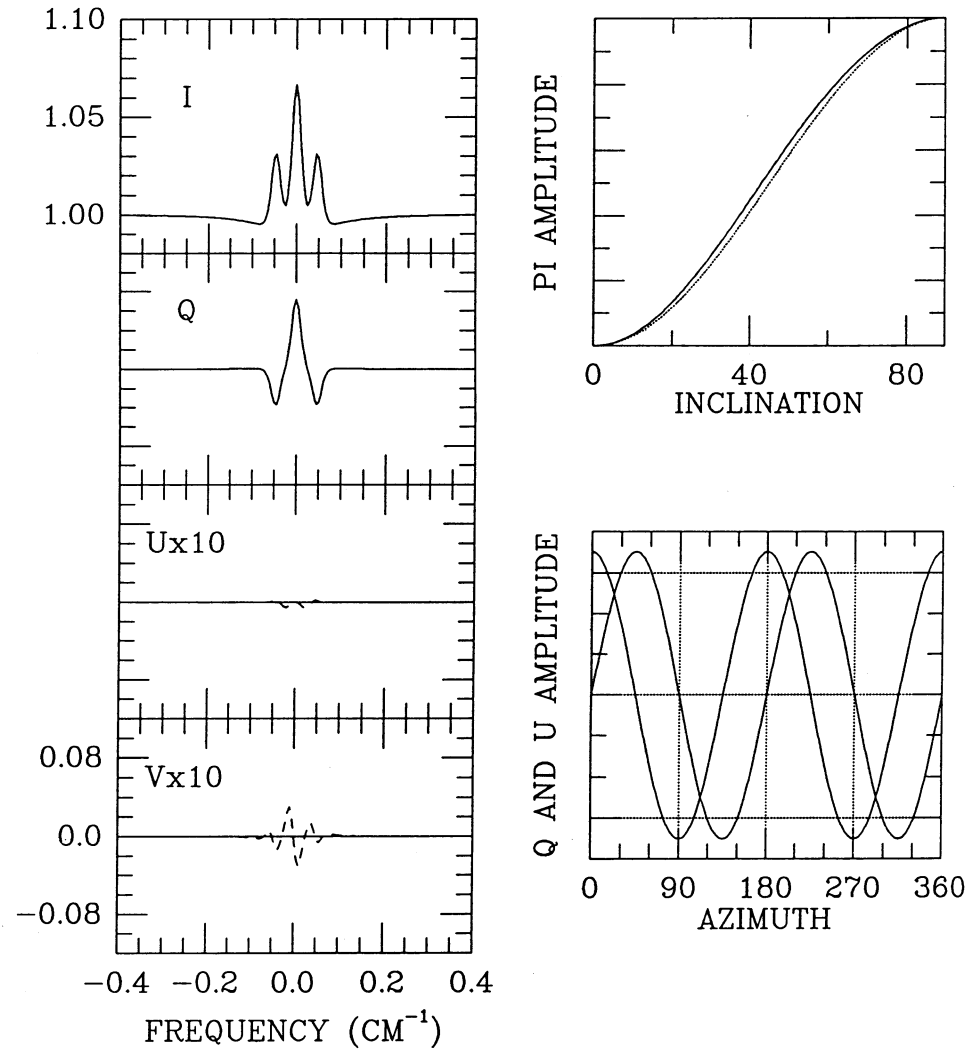

Fig. 4. Results of radiative transfer calculations for the Stokes profiles of the 12.32-μm lines. The I, Q, U, and V profiles on the left were calculated for a field inclination of 90° (*i.e.*, horizontal) and an azimuth of 0°. The dashed line shows the result of including magneto-optical effects (note the expanded scales for U and V). The π-component amplitude in the upper right includes the effects of magneto-optics, and is shown in comparison to a sin-squared relation (dotted line). The Q and U amplitudes in the lower right panel also include the effect of magneto-optics, which does not cause a significant perturbation in their azimuth dependence. All of the calculations were made for a field strength of 1,000 Gauss.

https://doi.org/10.1017/S0074180900124659 Published online by Cambridge University Press

The field inclination was taken to be 90° and the azimuth was 0°, putting all of the polarization signal into Stokes Q. The inclusion of magneto-optics (dashed lines) puts a small fraction of the polarization into Stokes V and Q, but the amount is so small that the effect is unimportant for vector field determinations at present. We also calculated the amplitude of the π component in Stokes Q and U as a function of field azimuth for 90° inclination (lower right), in order to test whether magneto-optics causes an apparent rotation of the azimuth. As is evident from the Figure, the angles of maxima and zeros of Q and U for the π component do not differ significantly from the values expected from the Seares relations. As a further test, we calculated the line-center amplitude of the π component as a function of field inclination (upper right), including magneto-optical effects. This relation is shown in comparison to the sin-squared dependence predicted from the Seares relation (dotted line). The maximum deviation from the sin-squared dependence amounts to less than 2°. We conclude from these calculations that the Hewagama (1991) Seares relation fits are adequate for the derivation of vector fields from the observed Stokes profiles.

4. Magnetic Configuration of Sunspots

Sunspots are the most prominent magnetic regions on the solar surface, so it is logical to apply the 12-μm lines first to sunspot studies. Several sunspots have now been observed at 12 μm (Deming *et al.* 1988; Hewagama *et al.* 1992), and some general conclusions have emerged. The dependence of magnetic field strength with distance from sunspot center has been observed in the visible by many authors (*e.g.*, Beckers and Schröter 1969), and this functional dependence is important as a test of magnetostatic sunspot theories (*e.g.*, Osherovich and Garcia 1989). Figure 5 shows this relation for two sunspots observed at 12 μm (Deming *et al.* 1988, Hewagama *et al.* 1992).

The first conclusion from these measurements is that azimuthal symmetry is a poor approximation for sunspot field strengths. The 12-μm splittings typically determine the field strength with an error of less than 50 Gauss, whereas the scatter in field strengths at a constant radius is several hundred Gauss, indicating that real azimuthal structure is present. Another point of interest is the value of the field strength at the penumbra/quiet Sun boundary, $R = R_p$. Beckers and Schröter (1969) concluded that the field at this boundary was half of the sunspot-center field strength, whereas Figure 5 shows that it is significantly less. The incomplete splitting exhibited in visible lines, in combination with the small field strength, and potential scattered light contamination at this boundary, have historically made this determination problematical. Indeed, some authors (Adam 1990; Wiehr and Balthasar 1989) have concluded that the magnetic field strength approaches *zero* a few arcseconds beyond this photometric boundary. The 12-μm data, however, show that the sunspot magnetic field extends to (typically) half a sunpot radius beyond the boundary with the surrounding photosphere ($R \sim 1.5R_p$). This conclusion is unequivocal, because the 12-μm splittings are resolved down to field strengths of 300 Gauss. The penumbral field at $R = R_p$ being 600 Gauss, scattered light cannot cause this to be confused with the 200–300 Gauss fields seen at $1.5R_p$. The

https://doi.org/10.1017/S0074180900124659 Published online by Cambridge University Press

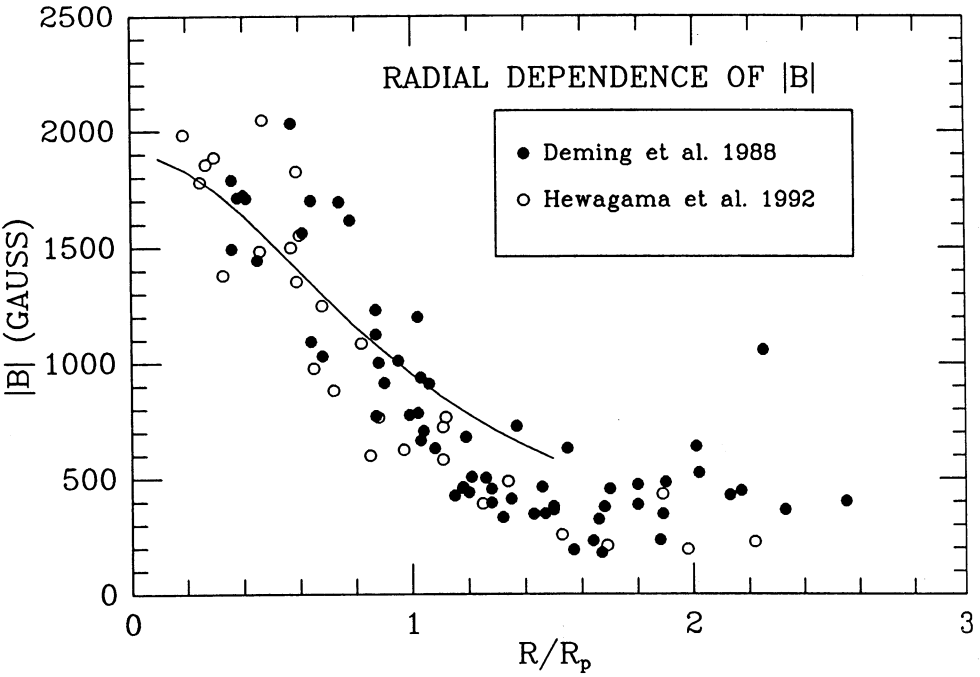

Fig. 5. Magnetic field strength versus distance from sunspot center in units of the penumbral radius, based on 12-μm measurements by Deming *et al.* (1988) and Hewagama *et al.* (1992). The solid line is the Beckers and Schröter (1969) relation.

conclusion that the field at $R = R_p$ is weaker than the Beckers and Schröter (1969) relation, but extends to a large fraction of a sunspot radius, is consistent with recent Stokes polarimetry in the visible (Lites and Skumanich 1990).

Parker (1979) has suggested that the sub-surface structure of sunspots in made up of a collection of discrete flux tubes separated by field-free gas. Since it is well known that sunspot penumbrae show filamentation in high-spatial-resolution images, it is natural to associate the filamentation seen in high-resolution images with magnetic filamentation. The 12-μm data can give us valuable insight into the possible intermittent nature of the sunspot field. Because the splitting is resolved, unpolarized radiation in the 12-μm π component can only arise as emission from field-free gas, not as the cancellation of orthogonal polarizations from incompletely-split σ components. Magnetic filling factors, based on the fraction of the 12 μm emission which is polarized, were derived by Hewagama *et al.* (1992) and are shown in Figure 6.

Within a mature sunspot, the 12-μm emission is essentially 100% polarized, decreasing to 90% at the boundary with the surrounding photosphere. This implies that field-free regions do not contribute significantly to the 12-μm sunspot emission, so the field at this altitude does not appear to be filamentary in the sense of being composed of discrete flux tubes separated by field-free gas. This conclusion is not

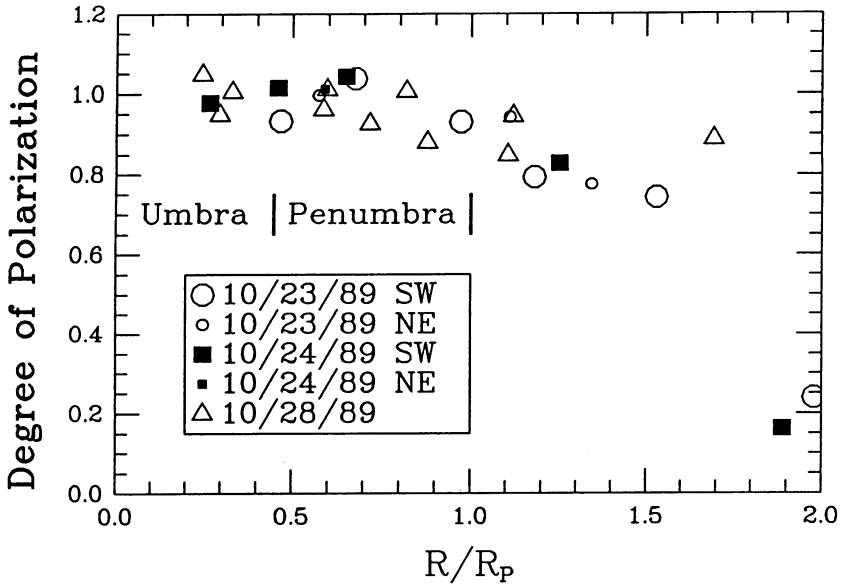

Fig. 6. Degree of polarization in the 12.32-μm line versus distance from sunspot center in units of the penumbral radius, from Hewagama *et al.* (1992).

surprising, since the lower gas pressure at the 12-μm altitude will allow discrete flux tubes to expand and merge.

The 12-μm data have also been used to deduce the inclination of the field to the surface normal, and Figure 7 shows this for a sunspot observed by Hewagama *et al.* (1992). The 12-μm inclinations in this instance differ considerably from the average values seen in the visible (see *e.g.,* Lites and Skumanich 1990). The smaller data symbols in Figure 7 represent a region of the sunspot which may have been affected by the presence of adjacent magnetic regions, and a filament. The inclinations to the surface normal are dramatically smaller in this region of the penumbra, which Hewagama *et al.* (1992) attribute to perturbation by the adjoining magnetic structure. While this seems plausible, visible observations have not shown such anomalies. Additional observations are needed in order to see whether inclination anomalies are a common feature in 12-μm data.

5. Progress Toward a 12-Micron Stokes Polarimeter

To date, most 12-μm magnetic observations have been made using the single-detector McMath FTS. Much could be learned about the magnetic configurations of solar active regions if 12-μm polarimetry were possible using a 2-D array detector. In addition to the magnetic configuration of sunspots discussed above, other outstanding problems in solar physics could benefit from such instrumentation. We note two examples of such problems:

https://doi.org/10.1017/S0074180900124659 Published online by Cambridge University Press

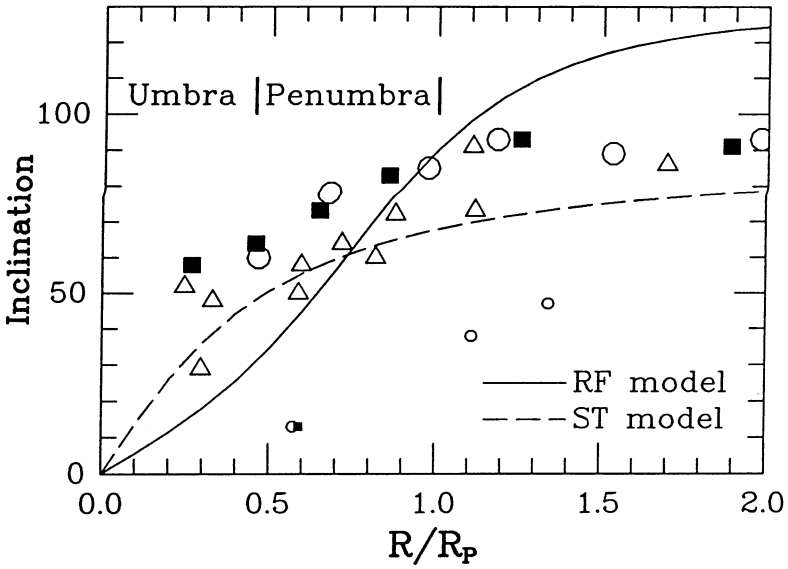

Fig. 7. The inclination of the magnetic field versus distance from the sunspot center in units of the penumbral radius. The inclinations are in heliographic coordinates, measured from a normal to the solar surface, in the 12.32-μm line by Hewagama *et al.* (1992).

(i) The Expansion of Plage and Network Flux Tubes. It has long been believed that most solar magnetic flux is present in strong-field form and that the relatively low field strengths seen by longitudinal magnetographs simply reflect the fact that the signal is diluted by the small filling factor for the magnetic elements. Rabin (1992) has used observations in the very Zeeman-sensitive 1.56-μm line to confirm the strong-field nature of plage flux tubes. His results also show spatially-resolved patterns in the field strength and filling factor. The field strength in an isolated thin flux tube varies with height as $\exp(-h/2H)$, where H is the gas pressure scale height. The factor $2H$ arises from the fact that the gas pressure difference between the flux tube and the surrounding photosphere is balanced by the magnetic pressure in the flux tube, the latter being proportional to $|\mathbf{B}|^2$. Over the 2.4 gas pressure scale heights which separate the 1.6- and 12-μm observations (125 to 400 km levels), the field strength should drop by a factor of 3.3. Plage field strengths at 12 μm are approximately 600 Gauss (Brault and Noyes 1983; Zirin and Popp 1989), whereas Rabin (1992) typically observes field strengths of 1400 Gauss at 1.6 μm. The observed field strength ratio of 1400/600 = 2.3 is less than expected by an amount which exceeds the errors in the IR observations. However, the 1.6- and 12-μm observations have, to date, not been simultaneous. Moreover, since Rabin observes a large-scale pattern in the field strengths, as well as filling factors as large as 30%, the real situation is doubtless much more complex than the thin-flux-tube model. Simultaneous vector field obser-

https://doi.org/10.1017/S0074180900124659 Published online by Cambridge University Press

vations over extended spatial scales at both 1.6 and 12 μm could tell us much about the manner in which plage fields are organized and their expansion with height.

(ii) Magnetic Field Relaxation Associated with Solar Fields. It is almost universally believed that the energy released in solar flares is extracted from that stored in non-potential magnetic field configurations (Haisch, Strong and Rodono 1991). However, observational proof of this belief has been difficult to obtain. It has been observationally established that flare occurrence is often associated with the existence of sheared photospheric fields (Hagyard *et al.* 1984). However, since the magnetic energy release occurs at coronal altitudes, its signature in photospheric magnetic observations is likely to be rather subtle. The approach which must be adopted is to calculate the magnetic free energy of an active region configuration, using photospheric observations as a boundary condition, and look for changes in this free energy which can be associated with a flare (Gary *et al.* 1987). Since this involves essentially an extrapolation of vector field measurements to coronal altitudes (Gary and Musielak 1992), the results are likely to be more robust if the vector fields are measured as high as possible. The upper photospheric nature of the 12-μm line, and its great magnetic sensitivity, suggest that 12-μm vector magnetograms would be excellent observational material with which to attack the flare problem.

We are developing a Stokes polarimeter for the 12.32-μm line, using IR array detectors. Array technology at this thermal IR wavelength is developing very rapidly. We are currently testing a 128 $\times$ 128 Si:As array from Rockwell as the detector for this polarimeter. The first decision which we made was that using a relatively large format array detector was impractical in an FTS, because the data rates would be impossibly high. Instead, the choice was between a grating spectrometer or a Fabry-Perot approach. There are really three dimensions to be observed, two spatial dimensions and one spectral dimension. Hence, we would ideally like to have a 3-D detector so as to observe all spatial positions and wavelengths simultaneously. Since we have at most a 2-D detector, we have to decide how to use it optimally. We could use one detector dimension spectrally, and the other spatially. This is the grating spectrometer approach with an input slit, and the slit has to be scanned in the remaining spatial dimension. The Near Infrared Magnetograph (NIM) being developed at NSO uses this method. Alternatively we could use both detector dimensions spatially, and scan the spectrum using a Fabry-Perot etalon. Since the Sun is significantly fainter at 12 μm than at 1.6 μm, the 12-μm observations take longer. Consequently, the efficiency with which we use the detector array is a greater concern. Measurements at approximately 50 points across a line are needed for adequate definition of Stokes profiles. The 128 $\times$ 128 array is already larger than this, so we gain in total efficiency by using both array dimensions spatially, and scanning an etalon through the spectrum.

The design of the 12-μm polarimeter is shown in Figure 8. Spectral resolution of 0.007 cm^{-1} is provided by a high-resolution etalon. It is scanned while maintaining parallelism using capacitance sensing of the plate separation and correction using

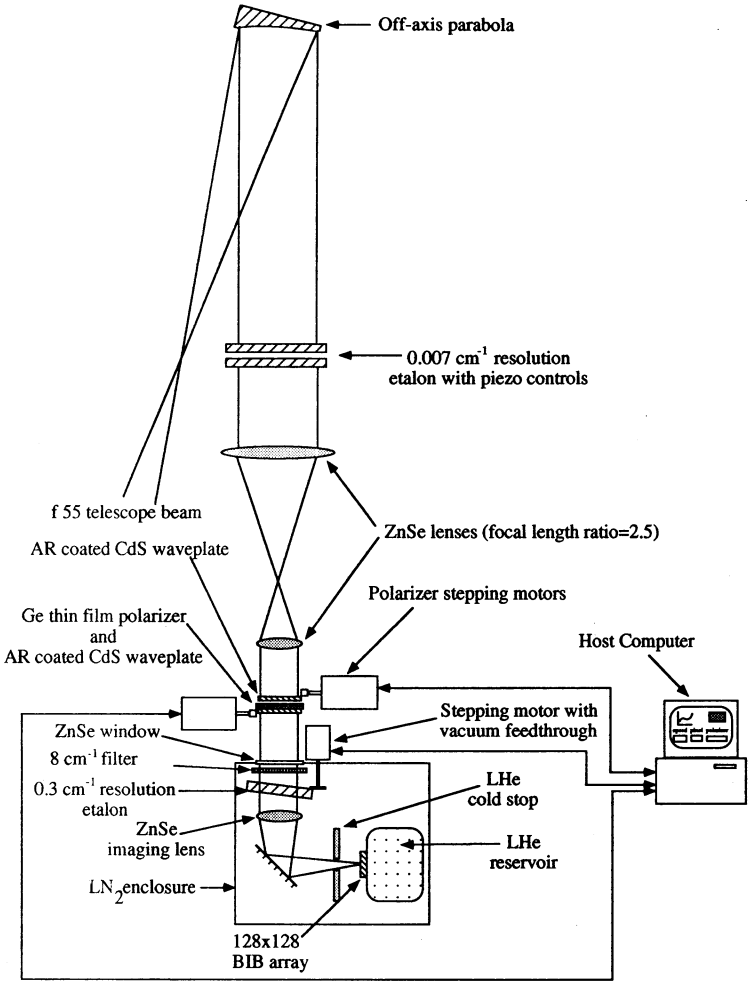

Fig. 8. Design of a 12-μm Stokes polarimeter using a 128 × 128 Si:As infrared array detector and Fabry-Perot etalons to provide spectral resolution.

piezoelectric actuators in a servo-loop. It was developed by Queensgate, Inc. and has a free spectral range of 0.4 cm^{-1}. A cold (LN_2) constant-gap etalon having a free spectral range of 8 cm^{-1} and resolution of 0.4 cm^{-1} is used to isolate a single high-resolution fringe. The lower-resolution etalon is mechanically tilt-tuned to follow the piezoelectric scanning of the high-resolution etalon. One low-resolution fringe is isolated using a narrow-band filter.

There are potential pitfalls involved in scanning the spectrum. The principal problem is likely to be changes in atmospheric transmission and instrumental sensitivity which are presumably $1/f$ in nature. The maximum read rate of the 128×128 array is 30 Hz, so almost two seconds are required to scan the spectrum. Figure 9 shows spectra taken using a very preliminary version of the 12-μm polarimeter,

https://doi.org/10.1017/S0074180900124659 Published online by Cambridge University Press

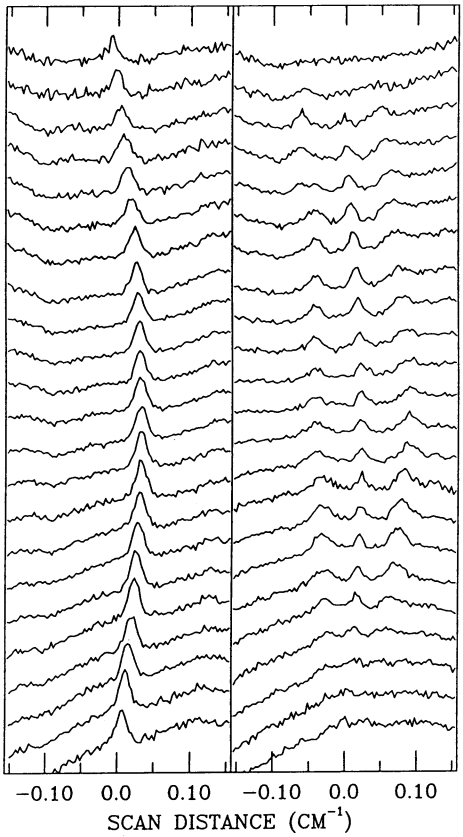

Fig. 9. Fabry-Perot-etalon spectra of the 12.32-μm line obtained using a very preliminary version of the Figure 8 polarimeter and a 24-element linear array detector. Quiet Sun spectra are illustrated on the left, and sunspot spectra on the right. Each spectrum corresponds to a single pixel of the 24-element array, viewing $3'' \times 3''$ on the solar disk.

scanning the spectrum even more slowly (about 30 seconds). This version used a 24-element linear array, rather than the 128 × 128. It also used a low resolution etalon which was uncooled, and its limiting noise level was determined by thermal background radiation from the warm etalon. The Figure 9 spectra show both a quiet-Sun region (left), and a sunspot region (right) where the line shows large splitting. The noise level in these test observations is considerably higher than will be possible when the low-resolution etalon is used cold. Nevertheless, it is encouraging that even the very slow scanning rate used for Figure 9 does not produce noise in excess of the thermal background from the warm etalon. When this thermal background noise is reduced, we may find that atmospheric and instrumental changes limit the observations. If so, the high-resolution etalon can be stepped to a reference continuum point on every other sample. This would double the observation time needed for the observations, but it would allow us to remove the effect of atmospheric and instrumental changes. We plan to generate Stokes profiles by

https://doi.org/10.1017/S0074180900124659 Published online by Cambridge University Press

subtracting successive measurements of $I + V$ and $I - V$, *etc.*, as described by Hewagama *et al.* (1992) for FTS data. The polarizers are rotated, under control of the data acquisition computer, using stepping motors.

The spectra shown in Figure 9 cover about 72″ on the solar disk (about 3″ per pixel). There is loss of finesse in the etalon for the pixels at each end of the linear array. The Figure 8 design will correct this by using a larger collimated beam through the high resolution etalon. The spatial resolution using the 128×128 array will be 0.8″ per pixel. This matches a single pixel to the diffraction-limited resolution of the proposed 4-meter McMath-Pierce telescope (Livingston 1991), and provides several-pixel sampling of its current resolution.

Acknowledgements

This work was supported by the NASA Solar Physics Branch, under RTOP 170-38-53-10. We thank Rockwell International for providing the 128×128 array, and Rob Rutten and Mats Carlsson for sending results of their calculations of source functions for the 12-μm lines.

References

Adam, M.G.: 1990, *Solar Phys.* **125**, 37.
Beckers, J.M., and Schröter, E.H.: 1969, *Solar Phys.* **10**, 384.
Brault, J.W., and Noyes, R.W.: 1983, *Astrophys. J. (Letters)* **269**, L61.
Carlsson, M., Rutten, R.J., and Shchukina, N.G.: 1991, *Astron. Astrophys.* **253**, 567 (CRS).
Chang, E.S.: 1987, *Phys. Scripta* **35**, 792.
Chang, E.S.: 1993, these proceedings.
Chang, E.S., and Noyes, R.W.: 1983, *Astrophys. J. (Letters)* **275**, L11.
Chang, E.S., and Schoenfeld,W.G.: 1991, *Astrophys. J.* **383**, 450.
Chang, E.S., Avrett, E.H., Mauas, P.J., Noyes, R.W., and Loeser, R.: 1991, *Astrophys. J. (Letters)* **379**, L79.
Deming, D., Boyle, R.J., Jennings, D.E., and Wiedemann, G.: 1988, *Astrophys. J.* **333**, 978.
Gary, G.A., and Musielak, Z.E.: 1992, *Astrophys. J.* **392**, 722.
Gary, G.A., Moore, R.L., Hagyard, M.J., and Haisch, B.M.: 1987, *Astrophys. J.* **314**, 782.
Hewagama, T.: 1991, Ph.D. Thesis, University of Maryland at College Park.
Hewagama, T., Deming, D., Jennings, D.E., Osherovich, V., Wiedemann, G., Zipoy, D., Mickey, D.L., and Garcia, H.: 1992, *Astrophys. J. Suppl.* in press.
Jennings, D.E., Deming, D., McCabe, G., Noyes, R., Wiedemann, G., and Espenak, F.: 1993, these proceedings.
Hagyard, M.J., Smith, J.B.Jr., Teuber, D., and West, E.A.: 1984, *Solar Phys.* **91**, 115.
Haisch, B., Strong, K.T., and Rodono, M.: 1991, *Ann. Rev. Astron. Astrophys.* **29**, 275.
Lites, B.W., and Skumanich, A.: 1990, *Astrophys. J.* **348**, 747.
Livingston, W.: 1991, *Proc. SPIE* **1494**, 50.
Maltby, P., Avrett, E.H., Carlsson, M., Kjeldseth-Moe, O., Kurucz, R.L., and Loeser, R.: 1986, *Astrophys. J.* **306**, 284.
Osherovich, V.A., and Garcia, H.A.: 1989, *Astrophys. J.* **336**, 468.
Parker, E.N.: 1979, *Astrophys. J.* **230**, 905.
Rabin, D.: 1992, *Astrophys. J. (Letters)* **390**, L103.
Rees, D.E., Murphy, G.A., and Durrant, C.J.: 1989, *Astrophys. J.* **339**, 1093.
Wiehr, E., and Balthasar, H.: 1989, *Astron. Astrophys.* **208**, 303.
Zirin, H., and Popp, B.: 1989, *Astrophys. J.* **340**, 571.